ENVIRONMENTAL RESEARCH
LETTERS

Permafrost sensitivity to global warming of 1.5°C and 2°C in the Northern Hemisphere

To cite this article before publication: Lei Liu *et al* 2020 *Environ. Res. Lett.* in press https://doi.org/10.1088/1748-9326/abd6a8

Permafrost Sensitivity to Global Warming of 1.5 °C and 2 °C in the Northern Hemisphere

L. Liu[1,2,4], D. Zhao[1], J. Wei[3], Q. Zhuang[4], X. Gao[1,2], Y. Zhu[1,2], J. Zhang[1,2], C. Guo[1,2], and D. Zheng[2]

[1]Key Laboratory of Land Surface Pattern and Simulation, Institute of Geographical Sciences and Natural Resources Research, Chinese Academy of Sciences, Beijing 100101, China.

[2]College of Resources and Environment, University of Chinese Academy of Sciences, Beijing 100101, China.

[3]Faculty of Geographical Science, Beijing Normal University, Beijing 100875, China.

[4]Department of Earth, Atmospheric, and Planetary Sciences, Purdue University, West Lafayette, IN 47907, USA

Corresponding author: Dongsheng Zhao (zhaods@igsnrr.ac.cn)

Abstract

Permafrost degradation induced by climate warming is widely observed in the Northern Hemisphere. However, changes in permafrost sensitivity to climate warming (PSCW) in the future remains unclear. This study examined the changes in permafrost distribution in the Northern Hemisphere under global warming of 1.5 ℃ and 2 ℃, and then characterized the spatial and temporal characteristics of PSCW. Global warming of 1.5 ℃ and 2 ℃ would result in 17.8±5.3% and 28.3±7.2% degradation of permafrost area under the climate scenario of Representative Concentration Pathway (RCP) 4.5, respectively, and 18.7±4.6% and 28.1±7.2% under the RCP 8.5, respectively. Permafrost tends to be more sensitive to climate change under the RCP 8.5 than RCP 4.5. PSCW shows small temporal variations in the 21st century under both RCPs, indicating a relatively stable sensitivity to warming on a hemisphere scale. However, PSCW varies greatly among regions, with high values at low latitudes and low values towards high latitudes. Air temperature is a major cause for the spatial heterogeneity of PSCW, explaining 66% of its variations. Permafrost under a warmer climate scenario tends to be more sensitive to the warming. Reducing snow depth and rising air temperature collectively enhances the permafrost sensitivity. Increasing in soil water content, by contrast, reduces the effect of warming. Permafrost in the south of the Northern Hemisphere is most vulnerable to climate warming. Our study highlights that permafrost in the region will respond differently under different warming scenarios across space (e.g., north vs. south) and time (e.g., summer vs. winter) in this century.

Keywords: permafrost, active layer, climate warming, temperature sensitivity, spatial and temporal variation

1 Introduction

Climate warming is more pronounced in cold regions of high altitudes (Pepin et al., 2015) and high latitudes (Huang et al., 2018; Cohen et al., 2014), leading to widespread permafrost degradation (Schuur et al., 2015; Romanovsky et al., 2010; Biskaborn et al., 2019; Meredith et al., 2019). It is estimated (Chadburn et al., 2017) that permafrost degradation due to global warming could be at $4.0^{+1.0}_{-1.1}$ million km^2/°C (1σ confidence). Permafrost thaw has far-reaching influences on environments and human society in cold regions. The downward moving of permafrost table and the drainage of thawed water can lead to the subside of ground surface, undermining the stability of human infrastructure, and changing landscape and hydrologic processes of surface and subsurface (O'Neill et al., 2019; Liljedahl et al., 2016). As a result, plant and soil microbial activities and consequent ecosystem processes can also be affected significantly (Pelletier et al., 2019; Wrona et al., 2016). The interaction of these physical, chemical, and biogeochemical processes in turn affect permafrost thermal regime (Loranty et al., 2018). It remains largely uncertain whether these interactions will accelerate or decelerate permafrost degradation caused by climate warming.

Increasing air temperature (*Ta*) contributes to permafrost degradation dominantly. During 1960-2009, changes in *Ta* contributed to 84% of the change in permafrost area (McGuire et al. 2016). Many model studies have examined the permafrost sensitivity to climate warming. For instance, Koven et al. (2013) calculated permafrost degradation in the 21st century using monthly predicted soil temperature with 18 CMIP5 models. They found there is a wide range of permafrost degradation rate, varying from 0.2 to 3.5 million km^2/°C. McGuire et al. (2016) also compared results of 15 models and found that permafrost area decreasing rate shows great differences among these models from 0.2 to 58.8 × 10^3 km^2/yr. The difference in complexity of the physical processes involved in these models and the lack of some critical processes such as thermokarst and ground ice dynamics, are the main reasons for these inconsistencies among models.

Field observations also showed that the influence of warming on permafrost state is uneven around the world. Observations from the circumpolar active layer monitoring (CALM) program showed there is a great spatial heterogeneity of the changing rate of active layer thickness (ALT) (Luo et al., 2016a). ALT decreased slightly at five sites, while the other 12 sites experienced distinct increasing trends, varying from 0.05 cm/a at Site U1 (Barrow) to 8.4 cm/a at Site K0 (Kazakhstan). Even under the same climate in a small basin, Sun et al. (2019) concluded that permafrost is more sensitive to warming at low elevations and sunny slopes. The different responses of permafrost (or ALT) to warming indicate that the sensitivity of permafrost to climate warming (PSCW) varies from sites to sites and regions to regions.

The difficulty in PSCW prediction and the variation of PSCW in observation is largely attributed to that climate warming does not affect permafrost thermal state directly. Heat from the atmosphere must be buffered by surface snow, plant, and soils, before affecting permafrost. Snow aggravates permafrost thaw by preventing cold air from penetrating into soils in winter and therefore keeping permafrost relatively warmer (Zhang, 2005). Vegetation does not affect permafrost temperature directly, but it can intercept snow and expose underlying soil to cold winter air. Organic soil layers and humus made of plant litters impact soil thermal properties considerably. Frost shade also has an influence on ground surface temperature (Loranty et al., 2018). The effects of water on permafrost temperature are complex. Wet soil has a higher thermal conductivity than dry soil. Therefore, heat conduction in wet soils is higher in summer. However, because of the

high heat capacity of water (4,200 J/kg℃), much more heat is needed to increase temperature in wet soils than in dry soils.

Although many studies have examined permafrost dynamics in the past and future, considering the influence of snow, vegetation, and soil properties, few studies have focused on PSCW directly, especially on the global scale. Our study adopted a semi-empirical model to analyze the spatial and temporal variations of permafrost responses to unit temperature change during the 21st century. This study shall increase our understanding of the dynamic responses of permafrost due to climate warming and help identify the most vulnerable permafrost zones to temperature increasing in the future.

2 Data and Methods

2.1 Methods

2.1.1 An overview of the GIPL model

We used the GIPL model (Sazonova & Romanovsky, 2003) to calculate active layer thickness (ALT) and mean annual ground temperature (MAGT). The core of the GIPL model is a modified Kudryavtsev's approach (Romanovsky & Osterkamp, 1997), which has several advantages over the classical Stefan equation (Shiklomanov & Nelson, 1999) and allows calculation of ALT and *Tps* under a wide variety of climate conditions (Anisimov et al., 1997). The GIPL model treats air, snow cover, surface vegetation, and active layer as separate layers with different thermal effects on the heat flow from the atmosphere to permafrost. This model has been evidenced to allow estimation of permafrost temperature with high accuracy in comparison with observations (within 0.5 ℃) (Sazonova et al., 2004), and has accurately estimated ALT in a broad range of permafrost regions, like Alaska (e.g., Shiklomanov & Nelson, 1999), Siberia (e.g. Romanovsky et al., 2007), and Qinghai Tibet Plateau (e.g. Luo et al., 2014). The model is driven by monthly *Ta*, precipitation, soil water content (*SWC*), and thermal properties of vegetation, snow cover, and soil layers (refer to Table S1 for all model input and output variables). MAGT is the same as mean annual temperature at the top of permafrost (T_{ps}) for regions where permafrost underneath, or mean annual temperature at the bottom of seasonal frozen layer. T_{ps} in GIPL model is given by eq (1):

$$T_{ps} = \frac{0.5T_{gs}\left(K_t + K_f\right) + A_{gs}\cdot\frac{K_t - K_f}{\pi}\cdot\left(\frac{T_{gs}}{A_{gs}}\arcsin\frac{T_{gs}}{A_{gs}} + \sqrt{1-\frac{T_{gs}^{\,2}}{A_{gs}^{\,2}}}\right)}{K^*} \tag{1-1}$$

$$K^* = \begin{cases} K_f, & \text{if numerator} < 0 \\ K_t, & \text{if numerator} > 0 \end{cases} \tag{1-2}$$

and ALT (Z) is calculated as eq (2):

$$Z = \frac{2\left(A_{gs} - T_{ps}\right)\cdot\left[\frac{K_t\cdot P\cdot C}{\pi}\right]^{1/2} + \frac{\left(2A_z\cdot C\cdot Z_c + Q_{ph}\cdot Z_c\right)\cdot Q_{ph}\left[\frac{K_t\cdot P_{sn}}{\pi\cdot C}\right]^{1/2}}{2A_z\cdot C\cdot Z_c + Q_{ph}\cdot Z_c + \left(2A_z\cdot C + Q_{ph}\right)\cdot\left[\frac{K_t\cdot P_{sn}}{\pi\cdot C}\right]^{1/2}}}{2A_z\cdot C + Q_{ph}} \tag{2-1}$$

$$A_z = \frac{A_{gs} - T_{ps}}{\ln\left[\frac{A_{gs} + Q_{ph}/2C}{T_z + Q_{ph}/2C}\right]} - \frac{Q_{ph}}{2C} \quad (2\text{-}2)$$

$$Z_c = \frac{2\left(A_{gs} - T_{ps}\right)\cdot\sqrt{\frac{K_t \cdot P \cdot C}{\pi}}}{2A_z \cdot C + Q_{ph}} \quad (2\text{-}3)$$

where T_{gs} and A_{gs} are annual mean ground surface temperature and annual amplitude, respectively (℃), accounting for the thermal influence of snow cover and surface vegetation. The calculation of T_{gs} and A_{gs} are documented by Sazonova and Romanovsky (2003) and have a brief description in the supplementary information. K_t and K_f are soil thermal conductivity in thawed and frozen state, respectively (W/m ℃). C is volumetric heat capacity of thawed ground (J/m^3 ℃, refer to Anisimov et al. (1997) for calculation), P is the period of the temperature cycle (1 year in second) and Q_{ph} is the latent heat of phase change (J/kg).

The 0 ℃ threshold of MAGT is critical for permafrost. When MAGT changes from negative to positive, the winter frozen front cannot reach permafrost table by the end of cold season, thus taliks begin to develop and permafrost starts to degrade. It should be noted that the GIPL model focuses on calculation of ALT and MAGT, but it does not calculate the unfrozen depth from ground surface, which includes ALT and the thickness of taliks. For the projection of permafrost area in this study, we excluded the regions where permafrost is already experiencing degradation (MAGT > 0 ℃).

There are some shortcomings of the GIPL model. First, it does not take into account unfrozen water and heat flows deeper into permafrost, which can play a critical role in permafrost thermal dynamics (Nicolsky & Romanovsky, 2018). Second, ground ice is another important factor that was missing but has significantly impacts on permafrost thermal state (Jorgenson et al., 2010; Jorgenson & Osterkamp, 2005). Besides, the GIPL model is an equilibrium model based on the assumption of a periodical, quasi-steady-state temperature regime (Kudryavtsev at al., 1974). The mean annual ground temperatures (MAGTs) calculated from the GIPL model fluctuate more greatly than measurements, and the difference between observed and calculated MAGTs can be as large as 1.5-2 ℃ (Sazonova et al., 2003). However, compared with transient models which have clear mechanisms but also require much more parameters, initial and boundary conditions, and model inputs that are difficult to acquire on a hemisphere scale, the equilibrium GIPL model demands much fewer model inputs and parameters and fit the needs of simulation on regional to continental and global scales (Luo et al., 2014; Anisimov et al., 1997; Anisimov and Reneva, 2006). Furthermore, when applied to decadal and longer time scales, the GIPL model shows an acceptable degree of accuracy of ±0.2~0.4 ℃ for the MAGTs and ±0.1~0.3 m for the ALT calculations. In addition, ALT and MAGTs calculated from the GIPL model show a strong correlation (r equal to 0.7~0.9, and p-value close to 0.0) with that calculated from transient models (Sazonova et al., 2003), demonstrating that the GIPL model is as efficient as transient models in detecting permafrost long-term changes.

In this study, we do not tend to predict the exact permafrost dynamics year by year. Instead, we pay more attention on long-term permafrost stability. The PSCW of each permafrost grid is calculated from all the Ta and ALT from 2006 to 2099 in that grid. Therefore, it actually represents the stability of the permafrost grids on a century scale. The projection of permafrost area under 1.5

and 2 ℃ of global warming is also based on decade average. Taken together, the equilibrium GIPL model shall be suitable for our research objectives.

2.1.2 Soil thermal conductivity

There are two key parameters in the GIPL, including soil thermal conductivity of thawed (K_t) and frozen (K_f) ground. Among many soil thermal conductivity models, the generalized thermal conductivity model developed by Côté and Konrad (2005) provided the best fit between estimation and experimental data (Barry-Macaulay et al., 2015). The generalized thermal conductivity model integrates the effects of porosity, degree of saturation, mineral content, grain-size distribution, and particle shape on the thermal conductivity of thawed and frozen soils. Soil thermal conductivity (K) of thawed and frozen ground is given below:

$$K = \left(K_{sat} - K_{dry}\right) \times K_r + K_{dry} \tag{3-1}$$

$$K_r = \frac{\kappa \cdot S_r}{1 + \left(\kappa - 1\right) \cdot S_r} \tag{3-2}$$

$$S_r = \frac{SWC}{100} \frac{\rho_d}{n \cdot \rho_w} \tag{3-3}$$

where K_{sat} and K_{dry} are thermal conductivity of saturated and dry soils (in thawed or frozen state), respectively (W/m ℃); K_r and S_r are the normalized thermal conductivity and the degree of saturation, respectively; κ is an empirical parameter used to account for the different soil types in the unfrozen and the frozen states (refer to Côté and Konrad (2005) for κ value); ρ_d and ρ_w are the density of dry soil and water (kg/m³), respectively; n is soil porosity. K_t and K_f were calculated using these equations separately, based on K_{sat}, K_{dry}, and SWC in thawed and frozen state, respectively.

2.1.3 Statistical analysis methods

The Geodetector method (Wang et al., 2010; http://www.geodetector.org/) was applied to calculate the contribution of different factors to the spatial distribution of PSCW. The method is based on the concept that the observations can be divided into strata (or categories and zones), within which the values are homogeneous but not between them. The stratified heterogeneity is related to the ratio between the variance within the strata and the pooled variance of the entire study area (Wang et al., 2016). q-statistic is used in this method to detect spatial stratified heterogeneity and to measure the association between independent factor (X) and dependent factor (Y), both linearly and nonlinearly. q-statistic is given as:

$$q = 1 - \frac{\sum_{h=1}^{L} N_h \sigma_h^2}{N \sigma^2} \tag{4}$$

where L is the number of stratum that Y composed of; N and N_h are the number of data points of Y and the stratum h, respectively; σ^2 and ${\sigma_h}^2$ are variance of the total Y and the stratum h, respectively. The strata of Y are a partition of itself, divided by an explanatory variable X, which should be stratified if it is a numerical variable. In this study, we stratified X (e.g. Ta) into 10 categories (L = 10) through the K-means method recommend by Wang and Xu (2017). The q-statistic can vary from 0 to 1, which means X explains q*100% of Y; q = 0 indicates that there is no coupling between Y and X; and q = 1 indicates that Y is completely determined by X. With definite physical meaning

and no linear hypothesis, this method has already been applied in many fields of natural and social sciences (Wang et al., 2010; Luo et al., 2016b; Zhang et al., 2019; Yang et al., 2020).

2.1.4 Calculation of permafrost sensitivity to climate warming

PSCW in this study was defined as the deepening of ALT upon 1 ℃ of warming. When plotting ALT against *Ta*, the slop of the curve is PSCW. To explore the temporal variation of PSCW in the 21st century, we plotted ALT against *Ta* in the three periods of 2010-2019, 2050-2059 and 2090-2099 (represent the beginning, middle and end of the 21st century), respectively. The temporal variation of PSCW was then deduced from the differences among the relation between ALT and *Ta* during these three periods. Spatially, we obtained PSCW for each permafrost grid by constructing a linear fitting equation for yearly ALT and *Ta* for 2006-2099 in that grid, and the slope of the fitted line is defined as PSCW for that grid. During the simulation, if *Tps* for a model grid exceeds 0℃, which means the surface permafrost is already thawed and a talik starts to form (Sazonova & Romanovsky, 2003), the calculated ALT for the grid at this time was set to null value (because the change of ALT in this case does not directly relate to the thermal dynamics of underneath permafrost below taliks). PSCW for the grid is then calculated from the remain ALT and *Ta* pairs. For model grids where there are few ALT and *Ta* pairs remain (less than 20 pairs), we did not calculate PSCW for them because small number of data pairs may cause great uncertainty during curve fitting and thus cannot get a robust PSCW. We also calculated the *p*-value (probability that the regression coefficient is zero) for the regression equation in each permafrost grid. If *p*-value in a model grid is greater than 0.05, we excluded PSCW for that grid.

2.2 Data

2.2.1 Climate data for model simulations

Climate data of monthly near-surface *Ta*, snowfall and soil moisture content were derived from four global circulation models (GCMs) in the second simulation round of the Inter-Sectoral Impact Model Intercomparison Project (ISI-MIP 2b). Known issues of previous round of ISIMIP have been solved for the ISIMIP2b through a series of adjustments, and atmospheric GCM data provided by the ISIMIP2b have also been bias-adjusted to a new reference dataset of EWEMBI (Frieler et al., 2017). The four GCMs (IPSL-CM5A-LR, GFDL-ESM2M, MIROC5, and HadGEM2-ES) provided a similar fractional range coverage to that of randomly chosen four-member sets of CMIP5 GCMs (Frieler et al., 2017). All climate variables have the same spatial resolution at 0.5°×0.5°, and the daily datasets were averaged to monthly. The temporal coverage of the datasets was 1986-2099. We used the historical (1986-2005) reconstruction climate data to drive our model and then validated the model results of permafrost distribution and ALT against previous studies and observations. For future (2006-2099) projections, Representative Concentration Pathway 4.5 (RCP 4.5) and RCP 8.5, which correspond to radiative forcing levels of 4.5 and 8.5 W/m^2 by 2100, respectively (Moss et al., 2010), were selected to evaluate the effects of climate change on PSCW. Data for the Southern Hemisphere were excluded.

It has been estimated that 1.5 ℃ and 2 ℃ warming threshold would be reached by about 2030 and 2050 under the RCP 4.5, respectively, and about 2025 and 2040 under the RCP 8.5, respectively (Karmalkar & Bradley, 2017; Li et al., 2019; Donnelly et al., 2017). To account for the uncertainties among different GCMs that were used to estimate the time threshold of 1.5 ℃ and 2 ℃ global warming, we adopted a 11-year span around each threshold year, that was 2025-

2035 and 2045-2055 for 1.5 ℃ and 2 ℃ warming under the RCP 4.5, respectively, and 2020-2030 and 2035-2045 for 1.5 ℃ and 2 ℃ warming under the RCP 8.5, respectively.

2.2.2 Snow depth, vegetation, and soil data for model simulation

Snow and vegetation property data are needed for the calculation of *Tgs* and *Ags*. Snow depth was calculated by the equation given by Nelson and Outcalt (1987) from monthly precipitation of the ISI-MIP 2b dataset. Snow thermal properties in this study were assumed constant over time and throughout the study area. ρ_{sn}, C_{sn}, and λ_{sn} were set equal to 300 kg/m^3, 0.32 W/m ℃ and 5.07×10^{-7} m^2/s, respectively (Shiklomanov and Nelson, 1999). Although these snow parameters are realistic for the whole northern hemisphere, they have much smaller effect on the model's overall accuracy than snow depth (Shiklomanov and Nelson, 1999). Because of the lack of vegetation thermal property data at the hemispheric scale, we assumed a 10 cm layer of moss across the study area with thermal diffusivity equal to 1.39×10^{-6} and 5.56×10^{-8} m^2/s in frozen and thawed states, respectively (Kudryavtsev et al., 1974). The 10 cm thick layer of moss has been proved to achieve the best fit against data from tundra regions by Anisimov et al. (1997).

Thermal conductivity of saturated and dry soils (K_{wet} and K_{dry}, respectively), and the density (ρ_d) and heat capacity (C_{dry}) of dry soil are needed during the calculation of K_f, K_t and C. The typical value for K_{wet}, K_{dry}, ρ_d, and C_{dry} of sand, silt, clay, and peat soil are given by Pavlov (1976) and Shiklomanov and Nelson (1999), showing good model performance when compared with observations (Anisimov et al., 1997; Shiklomanov and Nelson, 1999). For a given model grid, we first obtained the soil texture data for the grid from the Harmonized World Soil Database (v 1.2; FAO/IIASA/ISRIC/ISSCAS/JRC, 2012). Based on the soil texture data, we obtained the proportion of sand, silt, clay, and peat for that grid. By multiplying the proportion and corresponding thermal property and then summing up the results, we obtained the thermal property for that grid.

The lack of spatially explicit snow and vegetation thermal parameters on the hemisphere scale induces uncertainties in our model estimation. Additionally, this study did not consider the impacts of vegetation dynamics on permafrost degradation, which can be significant (Jorgenson et al., 2010; Loranty et al., 2018). Although enduring these uncertainties and the model shortcomings, by regressing ALT to *Ta* on a century scale, some fluctuations caused by these factors might have been filtered out, resulting in a robust estimation of the long-term PSCW trend.

2.2.3 Observed ALT data for model validation

Observed ALT from CALM network sites (https://www2.gwu.edu/~calm/data/north.htm) were used to validate the model results during the historical period (1986-2005). Three primary methods are employed at CALM sites. Some sites use spatially oriented mechanical probing at regular intervals across a grid (like 100 m × 100 m) and/or transect(s). Some sites employed thaw-tube measurements and some other sites infer thaw depth from ground temperature measurements. ALT is measured at the end of the thawing season each year. For spatially oriented measurements, ALT of the site is calculated by averaging all the sampling points at the site, while for point observations (e.g., thaw tube and ground temperature measurements), the single measurement is ALT for this site. In this study, we mainly chose the sites that employ the spatially oriented mechanical probing method to get a more general representation of the local value. The earliest ALT observation at CALM network sites can date back to 1990 and continue into present. But for the purpose of model validation of ALT during the historical period, we selected sites that have

sufficient (no less than 5) observations during 1990-2005. Sixty-five CALM sites (black dot in figure 1 (a)) around the Northern Hemisphere permafrost regions were finally selected. For the model validation, we first averaged the observed and calculated ALT from 1990 to 2005 to get the mean value for the historical period. Then located these 65 CALM sites into model grids and validated the model by comparing the historical mean ALT of the observations and model results in corresponding model grids.

3 Results

3.1 Model validation

Based on ISI-MIP 2b historical climate data, permafrost distribution in the Northern Hemisphere was simulated for the recent past (1986-2005, figure 1(a)). Permafrost extent in this study only includes regions where MAGTs are negative ($T_{ps} < 0$). According to Obu et al. (2019), the 0 ℃ of MAGTs roughly corresponds to the boundary of the discontinuous and sporadic permafrost regions. It can be seen from figure 1(a) that the simulated permafrost regions well match the continuous and discontinuous permafrost distribution (Brown et al., 2002). Permafrost area was estimated to be $14.9\pm0.2\times10^6$ km^2 (figure 1a), which is within the range of $12.2\text{-}17.0\times10^6$ km^2 given by Zhang (2000), but a little larger than 13.9×10^6 km^2 estimated by Obu et al. (2019) using the same indicator of negative MAGTs at the top of permafrost. But because the study period of Obu et al. (2019; from 2000 to 2016) is later than the historical period (1986-2005), considering the climate warming from 1986 to 2016, the larger extent of our study could be reasonable.

The comparison between measured and calculated ALT was shown as figure 1 (b). The modeled ALT is generally higher than observed values, suggesting that the model might have slight warming biases.

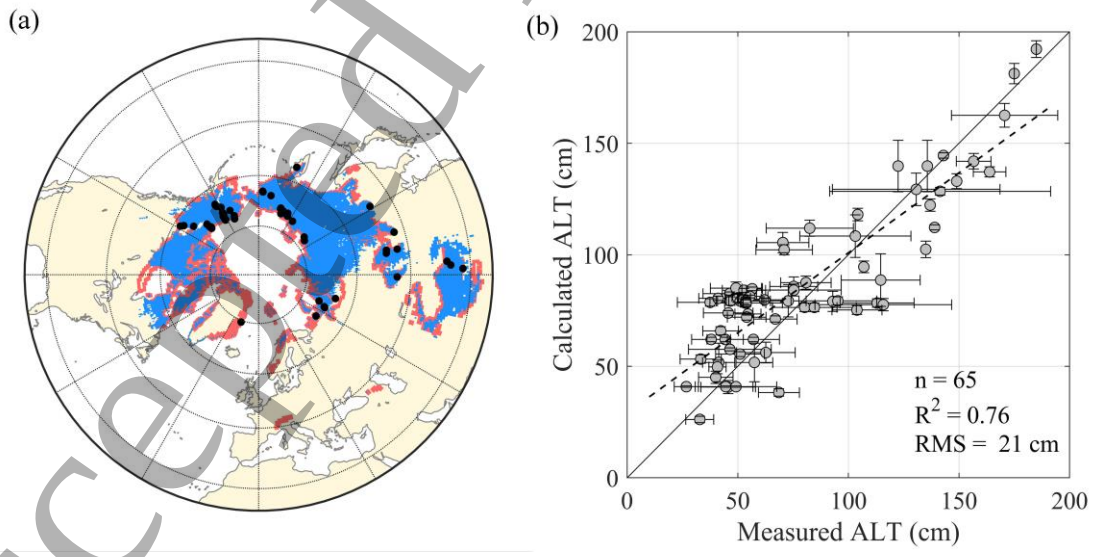

Figure 1. (**a**) Simulated permafrost distribution in the Northern Hemisphere under recent past climate (1986-2005) by GIPL model; the red lines denote the boundary of discontinuous and sporadic permafrost regions Brown's (2002) map. The black dots represent the location of the 65 observations from CALM, with averaged measured versus calculated ALT during 1995-2005 for

each site shown in (**b**). The horizontal and vertical error bars in panel (b) give the ± 1 standard deviation for measured and calculated ALT during 1990-2005, respectively.

3.2 Permafrost degradation in the 21st Century

All the four GCMs predicted a consistent warming during the 21st century under the two RCP scenarios (figure 2). The change of permafrost distribution is closely related to *Ta* changes. Under the RCP 4.5 scenario, when warming slows down after about 2070 for the IPSL-CM5A-LR and MIROC5 models, the decreasing in permafrost area would also decelerate. While under the RCP 8.5, persistent warming would lead to permafrost thaw continually. Among different models under the same RCP (figure 2), stronger warming would normally result in larger permafrost extent decrease, and vice versa.

We also estimated permafrost distribution when global mean *Ta* rises by 1.5 ℃ and 2 ℃ relative to pre-industrial levels (1850-1900), and permafrost distribution at the end of the 21st century (2090s) under the RCP 4.5 and RCP 8.5 scenarios, respectively (figure 3 and table 1). When *Ta* reaches the 1.5 ℃ warming threshold, 2.66±0.82 and 2.80±0.71 million km^2 of permafrost would thaw under the RCP 4.5 and RCP 8.5, respectively. Another 1.57±0.30 and 1.40±0.42 million km^2 of permafrost would thaw under the RCP 4.5 and RCP 8.5, respectively, when 2 ℃ warming threshold reached. Under both global warming threshold of 1.5 ℃ and 2 ℃, permafrost degradation rate is greater under the RCP 8.5 than RCP 4.5 (Table 1), indicating a higher sensitivity of permafrost extent to climate warming under the RCP 8.5.

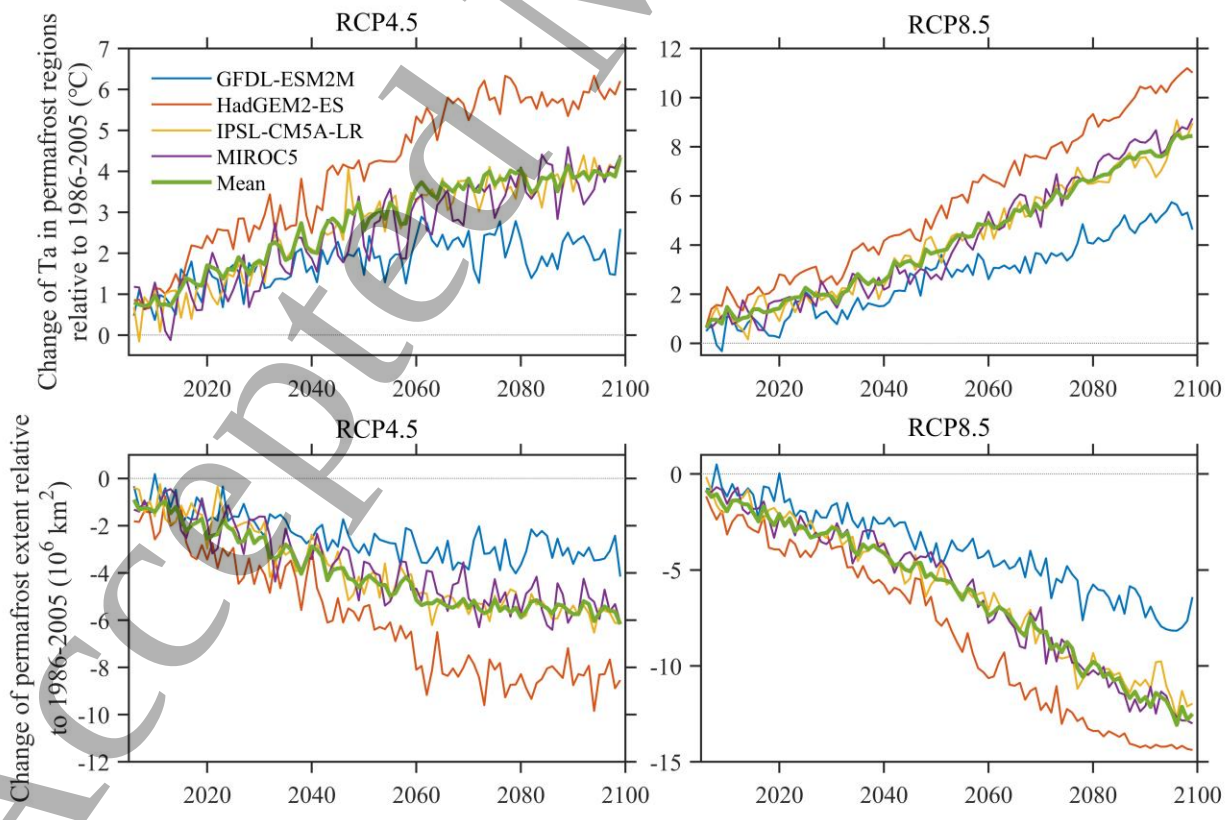

Figure 2. Changes in the Northern Hemisphere permafrost area and *Ta* in permafrost regions under the RCP 4.5 and RCP 8.5 scenarios, respectively.

By the end of the 21st century, *Ta* in permafrost regions would rise by 3.95±1.37 ℃ relative to present level (1986-2005) under the RCP 4.5, and the temperature sensitivity of permafrost distribution was projected at 1.47±0.08 million km^2/℃ during the 21st century. As a result, 39.3±11.9% (5.73±1.85 million km^2) of the present permafrost extent (14.9×10^6 km^2) would experience permafrost degradation. Under the RCP 8.5 scenario, only 24.1±15.2% of the current permafrost area would persist at the end of the 21st century, due to a much greater warming of 8.05±1.92 ℃ above present level. These permafrost regions would mainly distribute in northern Canada and in the east of Siberia inside the Arctic Circle (figure 3).

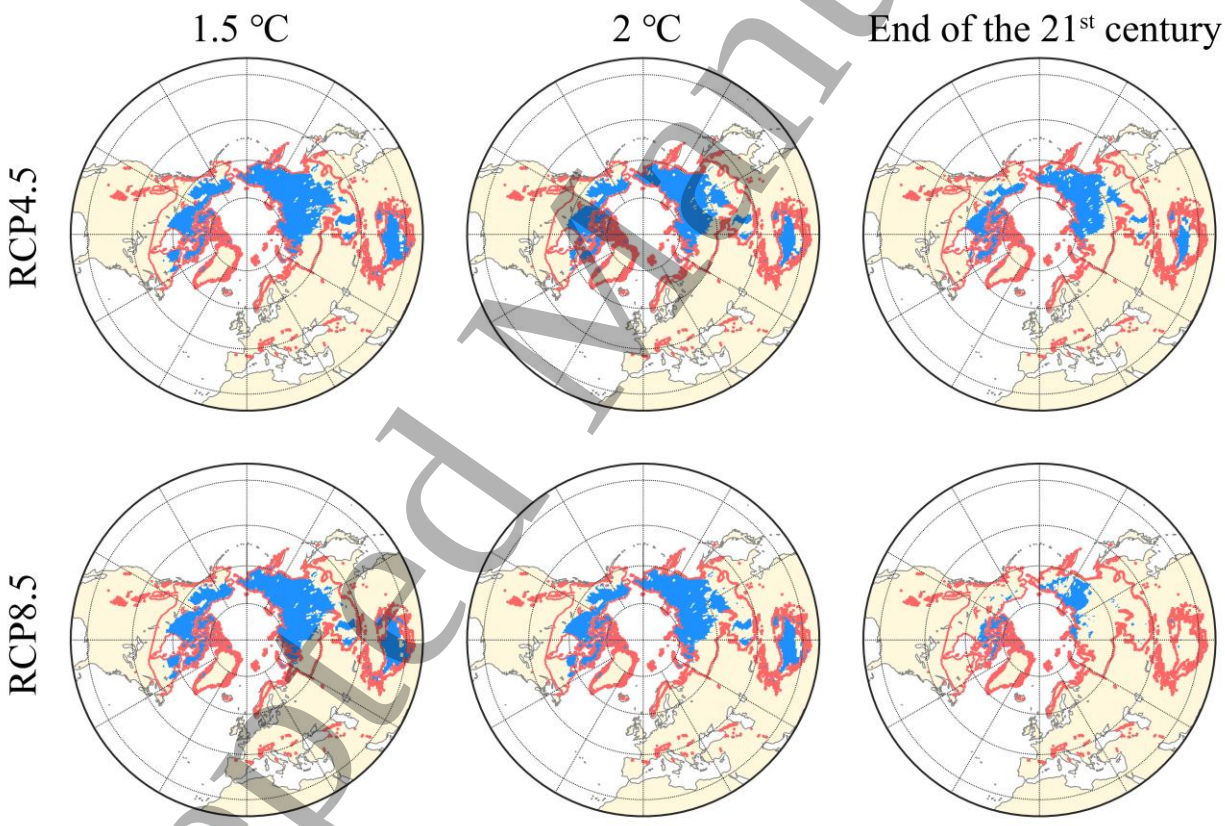

Figure 3. Distribution of the Northern Hemisphere permafrost when global mean near surface *Ta* rise by 1.5 ℃ and 2 ℃ above pre-industrial levels (1850-1900) and at the end of 21st century under the RCP 4.5 and RCP 8.5 scenarios respectively. Also shown in thick red lines are the boundary of the permafrost map provided by Brown et al. (2002).

Table 1. Projected Permafrost (PF) Extent in the Northern Hemisphere when global mean near surface *Ta* rise by 1.5 ℃ and 2 ℃ above pre-industrial levels (1850-1900), and at the end of the 21st century.

	1.5 ℃		2 ℃		End of the 21st century	
	RCP 4.5	RCP 8.5	RCP 4.5	RCP 8.5	RCP 4.5	RCP 8.5
PF degradation ($\times10^6$ km^2)	2.66±0.82	2.80±0.71	4.23±1.13	4.20±1.13	5.73±1.85	11.33±2.39
Remain fraction	0.82±0.05	0.81±0.05	0.71±0.07	0.72±0.07	0.61±0.12	0.24±0.15
Warming** (℃)	1.85±0.52	1.89±0.54	2.91±0.81	2.83±0.84	3.95±1.37	8.05±1.92
PF degradation per degree ($\times10^6$ km^2/℃)	1.43±0.13	1.48±0.09	1.45±0.07	1.48±0.07	1.47±0.08	1.42±0.05

Note. The second number in each cell is the standard deviation (*std*) for the four GCMs. ** denotes warming in permafrost regions relative to the regional mean *Ta* of 1986-2005.

3.3 Temporal and spatial variation of PSCW

To analyze the temporal and spatial variation of PSCW, we plotted ALT against mean annual, summer (May to October), and winter (November to April in the next year) *Ta* for all the Northern Hemisphere permafrost grids in three periods of 2010-2019, 2050-2059, and 2090-2099, respectively (figure 4). We used these three periods to represent the begin, middle, and end of the 21st century. Because of the degradation of permafrost, there are less data points for the period of 2090-2099 (as shown in the figure), especially for the RCP 8.5. On the hemisphere scale, ALT increases exponentially with mean summer *Ta*, leading PSCW, the slope of the fitted curves, increasing with mean summer *Ta*. However, the relationship between ALT and *Ta* is not clear in winter, and therefore resulting in a weak relationship for all year around. These results indicate that ALT is sensitive to temperature increase in summer but resistant to winter warming.

The differences in the slopes of the fitted curves at low and high summer *Ta* show that PSCW has great spatial heterogeneity in the Northern Hemisphere. As for temporal variation, there are little differences between the fitted curves of the three periods under the RCP 4.5. Although under the RCP 8.5, PSCW increases slightly during 2050-2059, compared to spatial heterogeneity, the differences of PSCW in the three periods are relatively small, indicating that the temporal variation of PSCW is relatively stable on the hemisphere scale.

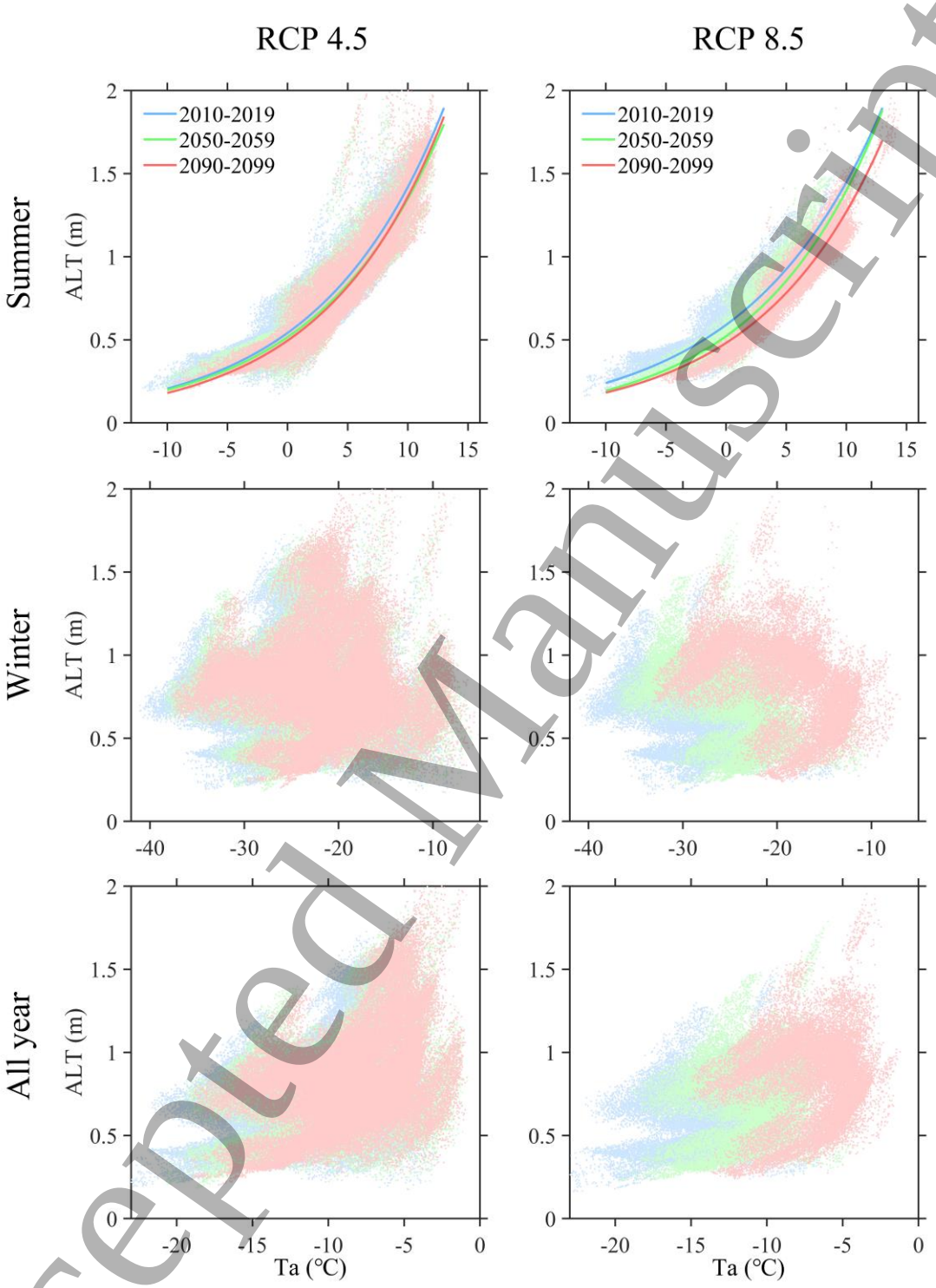

Figure 4. Scatter plot of ALT against mean annual, summer (May to October), and winter (November to April in the next year) *Ta* of all Northern Hemisphere permafrost grids during the 3 periods of 2010-2019, 2050-2059, and 2090-2099 under the RCP 4.5 and RCP 8.5, respectively.

The spatial distributions of PSCW based on mean annual, summer and winter *Ta* under the RCP 4.5 and RCP 8.5 are shown in figure 5, respectively. For all the distributions, PSCW are greatest in low latitudes and decrease with increasing latitudes. Furthermore, PSCW based on summer temperature is generally higher than that based on mean annual temperature, while PSCW based on winter temperature is the lowest. This phenomenon demonstrates again that ALT is more sensitive to summer warming. It should also be noted that although PSCW based on winter temperature is generally small, temperature increasing in winter still deepens ALT, especially for low latitude permafrost regions under the RCP 8.5 scenario.

As for the difference in PSCW under the two RCP scenarios, ALT tends to be more sensitive to warming (on matter it is annual, summer, or winter warming) under the RCP 8.5 (the histograms of figure 5), since more permafrost grids have higher PSWC under the RCP 8.5.

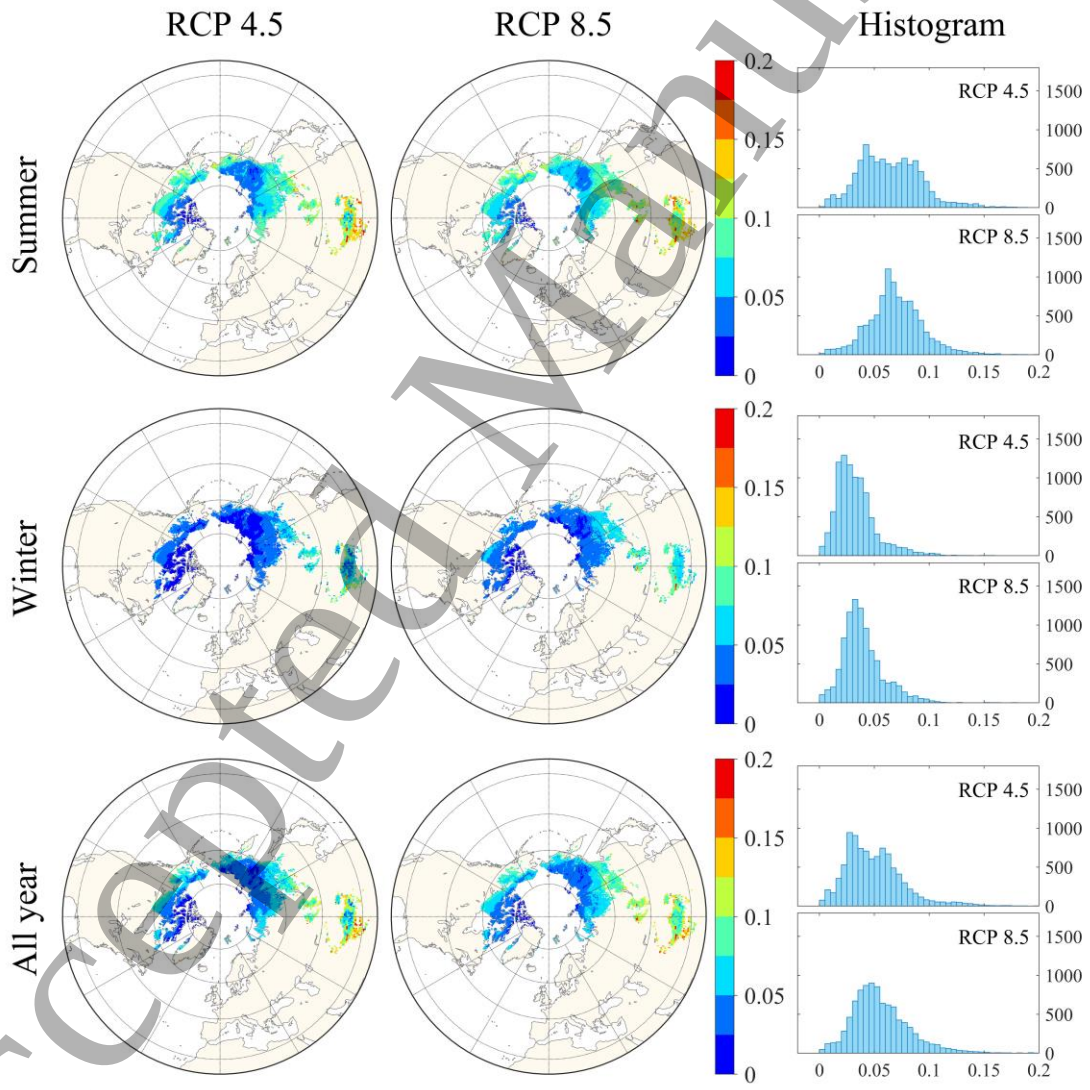

Figure 5. Distribution and histogram of PSCW (m/℃) based on mean annual, summer, and winter *Ta* in the 21st century under the RCP 4.5 and RCP 8.5 scenarios.

4. Discussion

4.1 Sensitivity of ALT and PSCW

We used a simplified method to examine the sensitivities of ALT and PSCW to *Ta*, seasonal air temperature amplitude (*Aa*), soil water content (*SWC*), and snow depth (*Zsn*), respectively. Take *Ta* as an example, first, we run the model with the original data of the RCP 4.5 scenario. Then we kept variables of *Aa*, *SWC* and *Zsn* unchanged but increased *Ta* in all the model grids during the whole study period by 0.5 ℃ at each step. The responses of ALT and PSCW to increasing temperature then can be plotted out (as shown in figure 6). The sensitivities of ALT and PSCW to *Aa*, *SWC*, and *Zsn* were also tested respectively (figure 6) using the same method (but with different steps: 0.5 ℃ for *Aa*, 0.02 for *SWC*, and 0.04 m for *Zsn*). Because in some regions, permafrost thaws quickly before the sensitivity study finishing (especially for increasing *Ta*), making the calculation of ALT and PSCW based on different permafrost extent, thus the comparison between different steps is not ideal. Therefore, we selected eastern Siberia (60°-75° N, 120°-150° E), which persists during all the simulation periods, as a representative region for this sensitivity study.

Both ALT and PSCW increase quickly with *Ta* (figure 6). The influence of *Ta* on ALT is direct, through deepening ALT in summer and increasing soil temperature and unfrozen soil water content in winter (Li et al., 2018). The increasing of PSCW with *Ta* means that ALT would deepen greater under warmer climate, suggesting that ALT is more sensitive to *Ta* in warmer climate. This can result from several processes. First, soil temperature would be relatively higher in a warm winter (Hansen et al., 2014), which can make the frozen ground easier to thaw during the coming spring and summer. Second, a warmer summer would transfer more heat into soil and compel permafrost table to move to a lower level. Moreover, freezing front moves shallower underground in a warmer winter. When freezing front cannot reach the permafrost table, talik will form between them and help thaw the surface frozen ground form bottom to up in next summer (Walvoord & Kurylyk, 2016).

ALT increased gradually with *Aa* even when *Ta* remained unchanged (figure 6). However, the influence of *Aa* on PSCW is limited. The increasing of *Aa* with *Ta* remaining unchanged means a warmer summer but a colder winter. A warmer summer under greater *Aa* would lead to the deepening of ALT, but a cold winter would decrease the soil temperature and unfrozen water content, which may improve the resistance of the frozen ground to temperature increasing in the next spring and summer and somewhat offset the warming effects on PSCW in summer, resulting in a limited influence on annual scale.

ALT and PSCW decrease with *SWC* noticeably (figure 6). Because of the high volumetric heat capacity of water, soil volumetric heat capacity will increase with *SWC* significantly. Therefore, it needs more heat to increase 1 ℃ of temperature in wet soils than dry ones, which makes wet soils more resilient to warming.

Zsn has important effects on permafrost thermal regime (Zhang, 2005; Park et al., 2015; Bisht et al., 2018). Because a large fraction of snow layer is filled with air, snowpack has extremely

low thermal conductivity, insulating thermal transfer between the atmosphere and substrate ground. With the increasing of snow depth, insulation effects of snowpack will be stronger than albedo effects (Zhang, 2005), warming the ground and therefore increasing both ALT and PSCW (figure 6).

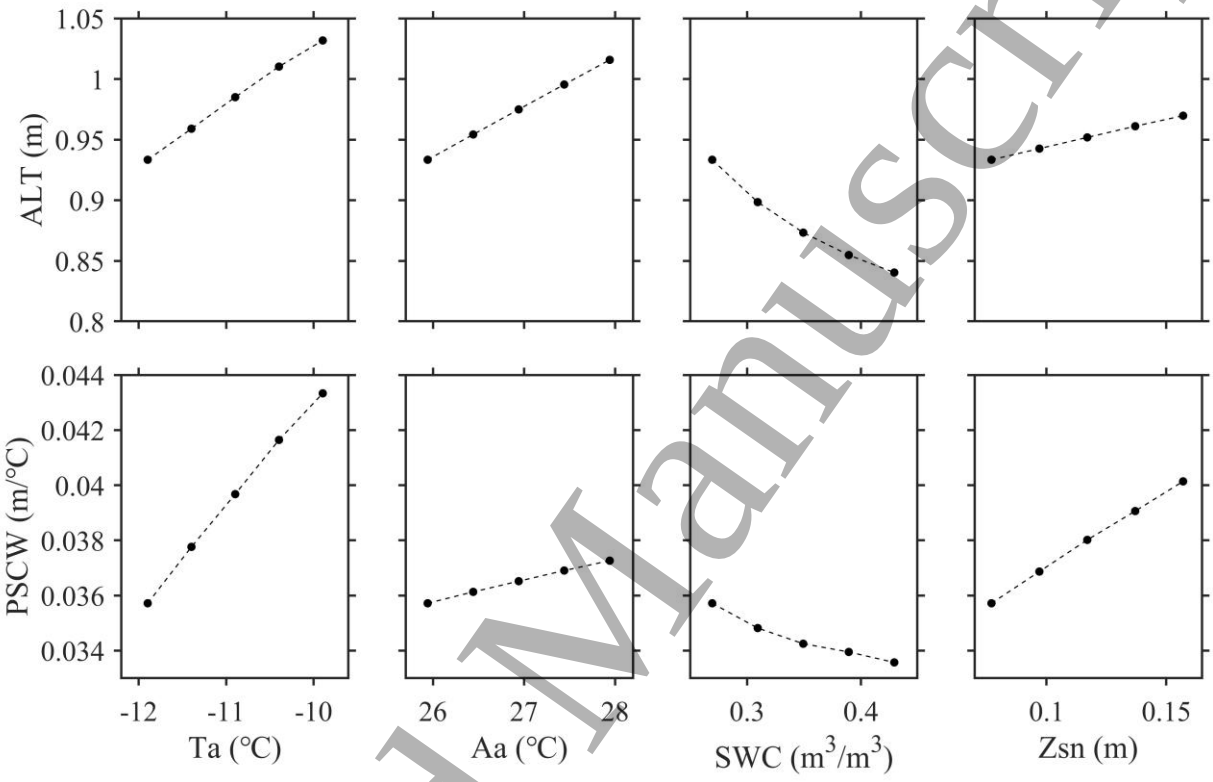

Figure 6. Sensitivity study of ALT (m) and PSCW (m/°C) for a representative permafrost region in Siberia (60°-75° N, 120°-150° E). The first dot (from left to right) in each panel is the calculated ALT or PSCW from original RCP 4.5 data. The dots (from left to right) after the first one was calculated from gradually increased *Ta* (°C), *Aa* (°C), *SWC* (m^3/m^3), or *Zsn* (m), respectively. *Ta* and *Aa* increase by 0.5 °C at each step; *SWC* increase by 0.02 at each step; and *Zsn* increase by 0.04 m at each step.

4.2 Temporal stability of PSCW

Figure 4 shows that although PSCW would change over time, their differences among the three periods (i.e., the three fitted lines) are relatively small. When plotting mean ALT against *Ta* in the Northern Hemisphere permafrost regions during 2006-2035, 2036-2065 and 2066-2095 (figure 7), we find that PSCW (the slop of ALT against *Ta*) are similar during these three periods, no matter based on mean annual *Ta*, or mean summer and winter *Ta*.

The dynamics of PSCW can be controlled by heat balance between the atmosphere and ground, and local factors such as vegetation, snow covers, soil thermal properties, surface water and groundwater. As for the temporal variation of a specific region, factors like topography and

soil texture can be treated as constant values in the 21st century. And since vegetation dynamics in the 21st century is out of the scope of this study and may introduce additional uncertainty, we fixed vegetation properties and focused mainly on the dynamics of *Ta*, *SWC*, and *Zsn*.

During the 21st century, *Aa* of the Northern Hemisphere permafrost region would decrease by 1.33±0.94 ℃ and 3.29±1.74 ℃ under the RCP 4.5 and RCP 8.5, respectively (figure S1). *SWC* and *Zsn* would increase by 0.02±0.0 and 0.01±0.00 m, respectively, under the RCP 4.5, and 0.03±0.02 and 0.02±0.0 m, respectively, under the RCP 8.5. The sensitivity study (figure 6) shows that the magnitude of the changes in *SWC* and *Zsn* under both RCPs would have limited influence (less than 0.002 m/℃) on PSCW. PSCW is sensitivity to *Ta* (figure 6). Figure 7 shows that PSCW tends to increase with summer warming under the RCP 8.5. However, since climate warming in permafrost regions would be more significant in winter (increasing by 4.42±2.36 ℃ and 11.25±3.89 ℃ under the RCP 4.5 and RCP 8.5, respectively) than in summer (increasing by 2.17±1.21 ℃ and 6.09±1.66 ℃ under the RCP 4.5 and RCP 8.5, respectively), and since PSCW is resistant to winter warming as described above, the relationship between ALT and *Ta* during the three periods on annual scale shows little variation (figure 7). Apart from this, although the decrease in *Aa* and the increase in *SWC* have limited influence on PSCW, both of them contribute to decreasing PSCW. As a result, PSCW would keep relatively stable on the hemisphere scale in the 21st century under both RCPs.

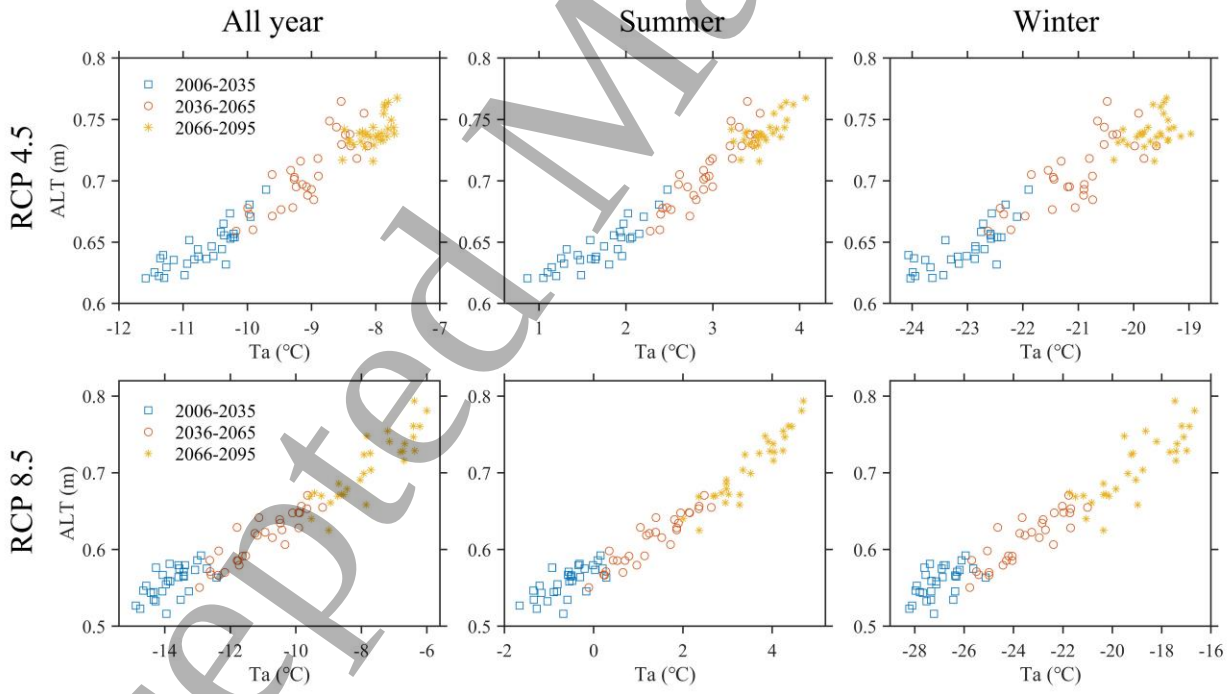

Figure 7. Relationship between mean ALT and mean annual, summer and winter *Ta* in three 30-year periods under the RCP4.5 and RCP 8.5, respectively

4.3 Spatial heterogeneity of PSCW

Figure 5 shows that PSCW would decrease significantly from low latitudes to high ones. We plotted the main impact factors of PSCW along latitude in figure 8. It can be seen that *Ta* shares the same spatial pattern of PSCW, while *Aa* and *Zsn* have opposite trends. *SWC* peaks at 55° - 60° N and then decreases slightly. Geodetector method results (Table S2) show that *Ta* could explain more than 50% of the spatial variation of PSCW, which is much greater than that of *Aa*, *SWC* and *Zsn* (about 10%, 14% and 14%, respectively). The variation of PSCW explained by *Ta* in this study is smaller than that in McGuire et al. (2016), which concluded that changes in *Ta* explain 84% of the change in permafrost area during 1960-2009. The difference may result from different study periods (historical vs. future), but the predominant role of *Ta* on permafrost dynamics is clear.

We further tested the sensitivity of PSCW to the spatial variation of *Ta*, *Aa*, *SWC* and *Zsn*. First, we set values of *Aa*, *SWC* and *Zsn* in all the pixels equal to their mean values between latitudes 45° - 50° N, respectively, but kept *Ta* the same as the original RCP 4.5 data. We run the model with these modified data and found that the calculated PSCW followed the original results (when *Ta*, *Aa*, *SWC* and *Zsn* all changes along latitude) (figure 8). This indicates again that *Ta* is the main reason for the spatial heterogeneity of PSCW, which is consistent with our Geodetector results.

In order to find out whether the spatial variation of *Aa*, *SWC* and *Zsn* would strengthen or weaken the effects of *Ta* on PSCW, we let one of the three variables (*Aa*, *SWC* and *Zsn*) change with *Ta* along altitude, but keep the other two equal to their mean values between latitudes 45° - 50° N. Figure 8 shows that when *Ta* and *Zsn* change together, PSCW is noticeably larger than that when *Ta* changes alone. This result demonstrates that *Zsn* would promote the influence of *Ta* on PSCW. However, *SWC* tends to have an opposite effect. Increased *SWC* in high latitudes tends to weaken ALT temperature sensitivity. *Aa* increases slightly with latitude and has weak regulation on the influence of *Ta* on PSCW.

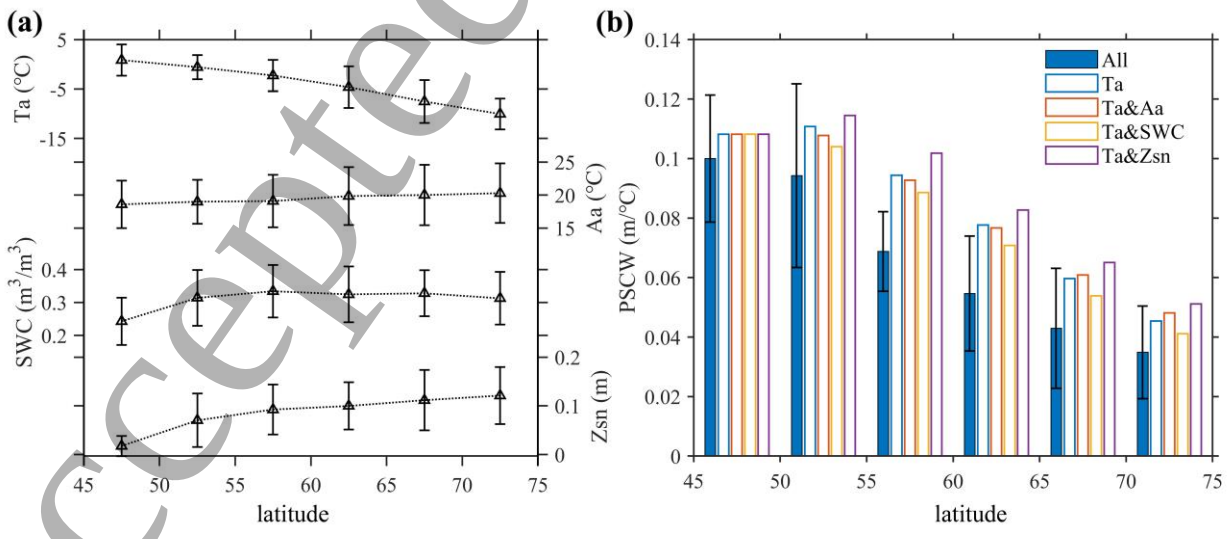

Figure 8. Variation of annual mean *Ta*, *Aa*, *SWC* and *Zsn* along latitude in Northern Hemisphere (**a**); PSCW along latitude (**b**). "All" indicates *Ta*, *Aa*, *SWC* and *Zsn* all varied along altitude as

RCP 4.5 scenario; "*Ta*" indicates only *Ta* varied along altitude as RCP 4.5, *Aa*, *SWC* and *Zsn* were set as their mean value of the latitude between 45°-50°N; "*Ta*&[*Aa*, *SWC* or *Zsn*]" indicates *Ta* and one of the three variables of [*Aa*, *SWC* or *Zsn*] changed along altitude while the other two variables were equal to their mean value of the latitude between 45°-50°N.

5. Conclusions

PSCW analysis is critical for understanding the dynamic responses of permafrost to climate warming. The spatial and temporal variation of the simulated PSCW in the Northern Hemisphere during 2006-2100 were analyzed. We found that, the 21st century would witness a wide permafrost degradation, starting from the south boundary towards high latitudes. Permafrost degradation would follow climate warming closely. Global warming of 1.5 ℃ and 2 ℃ relative to 1860-1900 would lead to 3.26±0.89 and 5.01±1.27 million km^2 of permafrost degradation, respectively, under the RCP 4.5, and 3.63±0.74 and 6.40±1.40 million km^2 of permafrost degradation, respectively, under the RCP 8.5. Permafrost is more sensitive to climate change under the RCP 8.5 than RCP 4.5.

PSCW shows small temporal variation on the hemisphere scale during the 21st century under both RCPs. The relatively small change in *Aa*, *SWC*, and *Zsn* and the mainly warming in winter (which has little influence on PSCW) may result in the temporal stability of PSCW. However, PSCW shows a great spatial heterogeneity, peaking at low latitudes and reducing towards high latitudes. *Ta* is the main factor affecting the spatial heterogeneity of PSCW, explaining more than 50% of its spatial variation. Permafrost in warmer climate tends to be more sensitivity to climate warming. Snow depth would interact with *Ta* to promote PSCW. But the regulation of *Ta* on PSCW tends to be weakened towards wet permafrost regions. The influence of *Aa* on the regulation of *Ta* on PSCW is relatively small.

Acknowledgments

This work was supported by projects of the 'Strategic Priority Research Program' of the Chinese Academy of Sciences (Grant No. XDA20020202) and the National Natural Science Foundation of China (Grant Nos 41571193 and 41530749). The research is also logistically supported by the Department of Earth, Atmospheric, and Planetary Sciences at Purdue University. We gratefully acknowledge financial support from China Scholarship Council. We thank three anonymous reviewers for their critical comments and suggestions. We also thank the ISIMIP cross sectoral science team for their roles in producing, coordinating, and making available the ISIMIP2b data (available at https://esg.pik-potsdam.de/search/isimip/). The authors declare no conflict of interest.

References

Anisimov O A, Shiklomanov N I and Nelson F E 1997 Global warming and active-layer thickness: results from transient general circulation models *Glob. Planet. Change* **15**(3-4) 61-77

Anisimov O A, Reneva S A 2006 Permafrost and changing climate: the Russian perspective. *Ambio* **35**: 169–175.

Barry-Macaulay D, Bouazza A, Wang B and Singh R M 2015 Evaluation of soil thermal conductivity models *Can. Geotech. J.* **52**(11) 1892-900

Bisht G, Riley W J, Wainwright H M, Dafflon B, Yuan F M and Romanovsky V E 2018 Impacts

of microtopographic snow redistribution and lateral subsurface processes on hydrologic and thermal states in an Arctic polygonal ground ecosystem: a case study using ELM-3D v1.0 *Geosci. Model Dev.* **11**(1) 61-76

Biskaborn B K, et al. 2019 Permafrost is warming at a global scale *Nat. Commun.* **10**(1) 264

Chadburn S E, Burke E J, Cox P M, Friedlingstein P, Hugelius G and Westermann S 2017 An observation-based constraint on permafrost loss as a function of global warming *Nat. Clim. Chang.* **7**(5) 340-+

Cohen J, et al. 2014 Recent Arctic amplification and extreme mid-latitude weather *Nature Geoscience* **7** 627

Cote J and Konrad J M 2005 A generalized thermal conductivity model for soils and construction materials *Can. Geotech. J.* **42**(2) 443-58

Donnelly C, Greuell W, Andersson J, Gerten D, Pisacane G, Roudier P and Ludwig F 2017 Impacts of climate change on European hydrology at 1.5, 2 and 3 degrees mean global warming above preindustrial level *Clim. Change* **143**(1-2) 13-26

Frieler K, et al. 2017 Assessing the impacts of 1.5 degrees C global warming - simulation protocol of the Inter-Sectoral Impact Model Intercomparison Project (ISIMIP2b) *Geosci. Model Dev.* **10**(12) 4321-45

Hansen B B, et al. 2014 Warmer and wetter winters: characteristics and implications of an extreme weather event in the High Arctic. *Environ. Res. Lett.*, 9(11): 114021

Huang J B, et al. 2018 Recently amplified arctic warming has contributed to a continual global warming trend (vol 7, pg 875, 2017) *Nat. Clim. Chang.* **8**(4) 345-

Jorgenson M T and Osterkamp T E 2005 Response of boreal ecosystems to varying modes of permafrost degradation *Can. J. For. Res.* **35**(9) 2100-11

Jorgenson M T, Romanovsky V, Harden J, Shur Y, O'Donnell J, Schuur E A G, Kanevskiy M and Marchenko S 2010 Resilience and vulnerability of permafrost to climate change *Can. J. For. Res.* **40**(7) 1219-36

Karmalkar A V and Bradley R S 2017 Consequences of Global Warming of 1.5 degrees C and 2 degrees C for Regional Temperature and Precipitation Changes in the Contiguous United States *PLoS One* **12**(1) 17

Koven C D, Riley W J and Stern A 2013 Analysis of Permafrost Thermal Dynamics and Response to Climate Change in the CMIP5 Earth System Models *J. Clim.* **26**(6) 1877-900

Kudryavtsev VA, Garagulya LS, Kondrat'yeva KA and Melamed VG 1974 *Fundamentals of Frost Forecasting in Geological Engineering Investigations* Cold Regions Reseach and Engineering Laboratory: Hanover, NH.

Li H, Yang Z and Wang J 2018 Unfrozen water content of permafrost during thawing by the capacitance technique *Cold Regions Science and Technology* **152** 15-22

Li Y, Tao H, Su B D, Kundzewicz Z W and Jiang T 2019 Impacts of 1.5 degrees C and 2 degrees C global warming on winter snow depth in Central Asia *Sci. Total Environ.* **651** 2866-73

Liljedahl A K, et al. 2016 Pan-Arctic ice-wedge degradation in warming permafrost and its influence on tundra hydrology *Nature Geoscience* **9** 312

Loranty M M, et al. 2018 Reviews and syntheses: Changing ecosystem influences on soil thermal regimes in northern high-latitude permafrost regions *Biogeosciences* **15**(17) 5287-313

Luo D, HuiJun J, Marchenko S and Romanovsky V 2014 Distribution and changes of active layer thickness (ALT) and soil temperature (TTOP) in the source area of the Yellow River using the GIPL model *Science China Earth Sciences* **57**(8) 1834-45

Luo D L, Wu Q B, Jin H J, Marchenko S S, Lu L Z and Gao S R 2016 Recent changes in the active

layer thickness across the northern hemisphere *Environmental Earth Sciences* **75**(7) 15
Luo W, Jasiewicz J, Stepinski T, Wang J F, Xu C D and Cang X Z 2016 Spatial association between dissection density and environmental factors over the entire conterminous United States *Geophys. Res. Lett.* **43**(2) 692-700
McGuire A D, et al. 2016 Variability in the sensitivity among model simulations of permafrost and carbon dynamics in the permafrost region between 1960 and 2009 *Glob. Biogeochem. Cycle* **30**(7) 1015-37
Meredith M, et al. 2019: Polar Regions. In: *IPCC Special Report on the Ocean and Cryosphere in a Changing Climate*
Moss R H, et al. 2010 The next generation of scenarios for climate change research and assessment *Nature* **463**(7282) 747-56
Nelson F E and Outcalt S I 1987 A Computational Method for Prediction and Regionalization of Permafrost *Arctic and Alpine Research* **19**(3) 279-88
Nicolsky D J and Romanovsky V E 2018 Modeling Long-Term Permafrost Degradation *Journal of Geophysical Research: Earth Surface* **123**(8) 1756-71
O'Neill H B, Smith S L and Duchesne C 2019 Long-Term Permafrost Degradation and Thermokarst Subsidence in the Mackenzie Delta Area Indicated by Thaw Tube Measurements *Cold Regions Engineering 2019* 643-51
Park H, Fedorov A N, Zheleznyak M N, Konstantinov P Y and Walsh J E 2015 Effect of snow cover on pan-Arctic permafrost thermal regimes *Climate Dynamics* **44**(9) 2873-95
Pelletier M, Allard M and Levesque E 2019 Ecosystem changes across a gradient of permafrost degradation in subarctic Quebec (Tasiapik Valley, Nunavik, Canada) *Arct. Sci.* **5**(1) 1-26
Pepin N, et al. 2015 Elevation-dependent warming in mountain regions of the world *Nat. Clim. Chang.* **5**(5) 424-30
Romanovsky V E and Osterkamp T E 1997 Thawing of the active layer on the coastal plain of the Alaskan Arctic *Permafrost Periglacial Process.* **8**(1) 1-22
Romanovsky V E, Sazonova T S, Balobaev V T, Shender N I and Sergueev D O 2007 Past and recent changes in air and permafrost temperatures in eastern Siberia *Glob. Planet. Change* **56**(3-4) 399-413
Romanovsky V E, Smith S L and Christiansen H H 2010 Permafrost thermal state in the polar Northern Hemisphere during the international polar year 2007–2009: a synthesis *Permafrost Periglacial Process.* **21**(2) 106-16
Sazonova T S and Romanovsky V E 2003 A model for regional-scale estimation of temporal and spatial variability of active layer thickness and mean annual ground temperatures *Permafrost Periglacial Process.* **14**(2) 125-39
Sazonova T S, Romanovsky V E, Walsh J E and Sergueev D O 2004 Permafrost dynamics in the 20th and 21st centuries along the East Siberian transect *J. Geophys. Res.-Atmos.* **109**(D1) 25
Schuur E A G, et al. 2015 Climate change and the permafrost carbon feedback *Nature* **520**(7546) 171-9
Shiklomanov N I and Nelson F E 1999 Analytic representation of the active layer thickness field, Kuparuk River Basin, Alaska *Ecol. Model.* **123**(2-3) 105-25
Sun A L, Zhou J, Yu Z B, Jin H J, Sheng Y and Yang C G 2019 Three-dimensional distribution of permafrost and responses to increasing air temperatures in the head waters of the Yellow River in High Asia *Sci. Total Environ.* **666** 321-36
Walvoord M A and Kurylyk B L 2016 Hydrologic Impacts of Thawing Permafrost-A Review

Vadose Zone J. **15**(6) 20
Wang J F, Li X H, Christakos G, Liao Y L, Zhang T, Gu X and Zheng X Y 2010 Geographical Detectors-Based Health Risk Assessment and its Application in the Neural Tube Defects Study of the Heshun Region, China *Int. J. Geogr. Inf. Sci.* **24**(1) 107-27
Wang, J F and Xu C D 2017 Geodetector: Principle and prospective *Acta Geographica Sinica* **72**(1) 116-134.
Wang J F, Zhang T L and Fu B J 2016 A measure of spatial stratified heterogeneity *Ecological Indicators* **67** 250-6
Wrona F J, Johansson M, Culp J M, Jenkins A, Mard J, Myers-Smith I H, Prowse T D, Vincent W F and Wookey P A 2016 Transitions in Arctic ecosystems: Ecological implications of a changing hydrological regime *J. Geophys. Res.-Biogeosci.* **121**(3) 650-74
Yang Y, Yang X, He M and Christakos G 2020 Beyond mere pollution source identification: Determination of land covers emitting soil heavy metals by combining PCA/APCS, GeoDetector and GIS analysis *CATENA* **185** 104297
Zhang L Q, et al. 2019 Air pollution exposure associates with increased risk of neonatal jaundice *Nat. Commun.* **10** 9
Zhang T 2005 Influence of the seasonal snow cover on the ground thermal regime: An overview *Reviews of Geophysics* **43**(4)
Zhang T, Heginbottom J A, Barry R G and Brown J 2000 Further statistics on the distribution of permafrost and ground ice in the Northern Hemisphere *Polar Geogr* **24** (2000) 126-131
Zhang Z Q, Wu Q H, Xun X Y and Li Y C 2019 Spatial distribution and changes of Xing'an permafrost in China over the past three decades *Quaternary International* **523** 16-24